Glyceraldehyde production by photocatalytic oxidation of glycerol on WO$_3$-based materials

Jie Yu,[a] Frederic.Dappozze,[a] Juan Martín-Gomez,[b] Jesús Hidalgo-Carrillo,[b] Alberto Marinas,[b] Philippe Vernoux,[a] Angel Caravaca,[a]* Chantal Guillard,[a]*

[a] Univ Lyon, Université Claude Bernard Lyon 1, CNRS, IRCELYON, F-69626, Villeurbanne, France

[b] Departamento de Química Orgánica. Instituto Universitario de Investigación en Nanoquímica (IUNAN). Universidad de Córdoba. Edf. Marie Curie (Annex). Campus de Rabanales, E-14071 Córdoba. España

E-mail: angel.caravaca@ircelyon.univ-lyon1.fr, chantal.guillard@ircelyon.univ-lyon1.fr

Abstract

Valorization of glycerol into high added-value products by photocatalysis can create, not only good economic benefits, but also cater to the global low-carbon and energy-saving environmental protection needs. In this study we proposed, for the very first time, to perform the photo-oxidation of glycerol towards added-value products with WO$_3$-based materials (homemade WO$_3$ and commercial WO$_3$/TiO$_2$ (DTW5)). Their performance was compared with that of state-of-the-art TiO$_2$-based photocatalysts (Anatase, Rutile, and P25). We found that, while TiO$_2$ favours the total oxidation of glycerol, WO$_3$-based materials exhibit an outstanding selectivity towards one of the most valuable oxidation products: glyceraldehyde. It was attributed to their enhanced acidity, which selectively activates C-O bonds in glycerol and facilitates the further desorption of glyceraldehyde to the liquid phase. This study establishes therefore a new starting point towards the development of advanced materials for an efficient valorization of glycerol.

Keywords: photocatalysis, valorization, glycerol, glyceraldehyde, WO3

1 Introduction

The current development of economy has nowadays a significant ecological impact. Therefore, the generation of clean energy, together with the production of high-value chemicals to replace the utilization of petroleum-derivate products via efficient/non-expensive technologies, have become a major challenge for human beings. In particular, the current energy sector in this

world mainly depends on limited sources of fossil fuels, which limits the long-term development of economy. Thus, the production of biodiesel fuel derived from a renewable biomass source has become one of the main strategic alternatives to overcome these issues. As a matter of fact, according to the report provided by the Food and Agriculture Organization of the United Nations (OECD/FAO), the production of biodiesel is increasing year by year and it is forecasted to remain at a high level [1], [2]. However, the production of biodiesel is accompanied with a significant co-production of glycerol. Around 100 kg of glycerol (∼110 kg of crude glycerol) are generated from 1 ton of biodiesel production [3], leading to a significant devaluation of this product on the market. As a consequence, an important amount of glycerol is finally incinerated for heat energy production. Nevertheless, considering that biomass is the only alternative to fossil fuels for production of chemicals, it would be more interesting to convert glycerol into value-added products. Therefore, a better valorization of glycerol will have great economical and environmental benefits.

Glycerol, with three hydroxyl groups, can be transformed into a wide variety of value-added products, including dihydroxyacetone, glyceraldehyde, glyceric acid, tartronic acid, glycolic acid, formic acid and oxalic acid [4],[5]. All these products, except for oxalic acid and formic acid, with high production volumes, are economically more interesting than glycerol. For example, glyceraldehyde could be applied in the domains of cosmetic and pharmaceutical industry as well as organic chemistry [6]. Dihydroxyacetone could be used in cosmetics as ingredient in tanning lotions [7]. Glyceric acid has found applications in the field of medicine to cure the skin disorders [8]. Glycolic acid could be utilized in daily necessities such as degreasing agent, tanning agent and skin care products [9]. Tartronic acid and oxalic acid are used as an agent of chelating in fine chemistry [10]. Nevertheless, among them, glyceraldehyde is one of the most value-added products [11], [12]. Thus, selective catalytic oxidation of glycerol to glyceraldehyde possesses great commercial value.

To achieve the production of high value chemicals, different technologies have been applied in glycerol oxidation, such as thermo- [13], [14], [15], photo- [16], [17], [18], electro- [19], [20], [21], and photoelectrocatalytic technologies [22]. Among them, photocatalysis is considered as a green and energy-saving technology which attracts scientists' attention all over the world, since it utilizes light (potentially sunlight) to generate charge carriers (holes and electrons) and active species, which can activate the target molecules [23]. In this sense, most photo-oxidation reactions usually take place at room temperature and atmospheric pressure, by using a semiconductor with the proper band gap to ensure a good potential application prospect. Since V. Maurino et al. [24] firstly reported the photocatalytic oxidation of glycerol as a possible route to produced added-value chemicals in 2008, many studies have been carried out to investigate this reaction over different catalytic materials. Most of them were performed on the most popular photocatalytic material, i.e., TiO_2. As an example, some of those works focused on the performance of glycerol oxidation over TiO_2 or TiO_2-doped with noble metals such as Au or Pt. [25], [26] V. Augugliaro and co-workers [27] used commercial and home-made TiO_2 samples in the anatase, rutile or anatase-rutile phases to investigate the glycerol oxidation products in an aqueous solution and showed that1,3-dihydroxyacetone (DHA), glyceraldehyde, formic acid and carbon dioxide are the main products. In their study, the highest selectivity of the value-added glyceraldehyde was 13% and that of DHA was 8% at a 35% glycerol conversion. C. Minero et al. [28] used two different commercial TiO_2 powders (Degussa P25 and anatase Merck TiO_2) to investigate the photocatalytic oxidation mechanism of glycerol and found that various TiO_2 specimens could lead to different selectivities of products.

WO_3 is an excellent metal oxide semiconductor photocatalyst [29], [30], with better visible light response than TiO_2. However, to the best of the authors´ knowledge, although it has been widely used in many fields such as H_2 evolution by glycerol electroreforming [31], [32], the

degradation of pollutants [33], gas sensor [34] and electrochemical energy storage [35], the photocatalytic oxidation of glycerol towards high-value chemicals has never been investigated on WO_3. Therefore, the aim of this work is to study and thoroughly characterize a series of WO_3-based materials for the photocatalytic oxidation of glycerol towards added-value chemicals. An outstanding performance was found towards the production of glyceraldehyde, one of the most valuable derivatives of glycerol. The activity and selectivity provided by such materials were compared with those of commercial TiO_2-based photocatalysts.

2 Experimental
2.1 Photocatalytic materials and photocatalytic activity measurements

Several WO_3- and TiO_2-based materials were used in this study. First of all, a pure WO_3 photocatalyst was prepared by a simple hydrothermal method. Firstly, 0.6 g of WCl_6 was dissolved in 120 mL of Ethanol solution under constant stirring at room temperature for 10 min. Then, the obtained solution was transferred to a Teflon-lined stainless-steel autoclave (200 mL) and kept in an oven for 12 h (180 ºC). Finally, after cooling down to room temperature, WO_3 powder was withdrawn, washed with Ethanol (3 × 90 mL) and deionized water (3 × 90 mL), and dried at 80 ºC in air over night. This material was tested as prepared. For comparison purposes, the as-prepared WO_3 catalyst was also calcined at 450 ºC.

In addition, a series of TiO_2-based materials were acquired commercially, including: Anatase (HPX-200), Rutile (HPX-400C) and DTW5 (5 wt% WO_3/TiO_2), all of them provided by Tronox®, while P25 (a very well-known heterojunction of anatase/rutile) was supplied by Evonik®.

A typical photocatalytic experiment was carried out according to the following protocol: 7.5 mg of the catalyst were introduced in a quartz reactor containing 30 mL of glycerol (in aqueous solution concentration of 1.10 mmol L^{-1}). The photocatalytic reactions were conducted under ultraviolet light with an UV lamp (UV-A PL-L, 18 W) which delivers an irradiation intensity

of 5.60 mW cm^{-2}. The reactor is open to the air without bubbling. Prior to the photocatalytic reaction, the suspension was stirred for 30 min in the dark to achieve the adsorption-desorption equilibrium of glycerol on the surface of catalysts Every 30 min, a sample (0.5 mL) was taken from the mixture solution and immediately filtered by a Millipore 0.45 μm (hydrophilic PVDF) membrane using a plastic syringe. In the case of WO$_3$, the sampling interval is 2 h and its photooxidation performance is tested by two parallel experiments owing to its low kinetic. The concentrations of glycerol and derivate products were analysed by a Shimadzu SPD-M20A prominence ultrafast high-performance liquid chromatograph (HPLC) assembled with a Transgenomic ICSep ICE-COREGEL-87H3 organic acid column. The mobile phase is 5 mmol/L of H$_2$SO$_4$ and its flow rate is 0.7 mL/min. The temperature of oven is 30 °C. The products of glycerol oxidation could be determined by the ultraviolet detector at the wavelength of 210 nm except from glyceric acid which is identified at 240 nm. Glycerol could be analyzed by the refractive index detector (RID).

The Glycerol conversion (in %) was calculated according to equation (1):

$$Glycerol\ conversion\ (\%) = \left(\frac{C_{0\ glycerol} - C_{t\ glycerol}}{C_{0\ glycerol}}\right) \times 100 \quad (1)$$

where $C_{0\ glycerol}$ and $C_{t\ glycerol}$ stand for the initial and real-time concentrations of glycerol, respectively.

The Yield (in %) of every product was calculated according to equation (2):

$$Yield\ (\%) = \left(\frac{C_{t\ product}}{C_{0\ glycerol}}\right) \times 100 \times n \quad (2)$$

where $C_{t\ product}$ stands for the real-time concentration of the product and n is the carbon number ratio of product versus glycerol.

The Selectivity (in %) of every product was calculated according to equation (3):

$$Selectivity\ (\%) = \left(\frac{C_{t\ product}}{C_{0\ glycerol} - C_{t\ glycerol}}\right) \times 100 \times n \quad (3)$$

where all the parameters were already defined in equations (1) and (2).

2.2 Characterization

X-ray diffraction (XRD) was conducted with a Bruker D8 diffractometer using Cu Kα (λ= 0.15406 nm) radiation equipped with 1-D fast multistrip detector (LynxEye, 192 channels on 2.95°) and a Ni filter. Other test conditions included a current of 100 mA, an operating voltage of 40 kV, a scanning range between 2θ = 4-80°and a scan rate of 0.02°/ s. Phase, crystallinity and average crystallite size identification were carried out using the Diffrac.Eva software (Bruker) and the ICDD-PDF4+ database.

Scanning electron microscopy (SEM) was conducted by FEI-XL30. Each sample was sprinkled on a conductive tape and sprayed with gold under a 15 kV work voltage. The high-resolution transmission electron microscopy (HRTEM) was performed on a JEOL-2010 microscope equipped with an EDX detector.

The Brunauer−Emmett−Teller (BET) surface area of the catalysts was measured via nitrogen adsorption at −196 °C (Micromeritics ASAP 2020). The catalysts were degassed at 160 °C for 3 h under vacuum. The porous volume and the pore size distribution were calculated via the Barrett-Joyner-Halenda (BJH) method.

UV-vis diffuse reflectance spectroscopy (UV-vis DRS) measurements were conducted using an AvaSpec-2048 Fiber Optic Spectrometer. Spectra were recorded from 200 to 600 nm using a 2048 pixel CCD detector array. Barium sulfate ($BaSO_4$) was used as a blank reference.

The electrochemical photocurrent experiments were carried out in a photoelectrochemical cell (supplied by redox.me ®) with a standard three-electrode system consisting of a Pt wire as the counter electrode, a saturated Ag/AgCl as the reference electrode and a working electrode prepared by the following process: 5 mg of the catalyst (as-prepared WO_3 or commercial samples) were dispersed in 0.5 mL ethanol. Then, 20 μL of that dispersion were impregnated over an indium-tin oxide (ITO) substrate, with an active area of ca. 1 cm^2, and dried at room

temperature. Different electrical potentials were applied with a potentiostat-galvanostat (VoltaLab PGZ402).

The concentrations of total organic carbon (TOC) of the solutions before and after the photocatalytic tests on different materials were measured using a Shimadzu TOC-VCPN analyzer equipped with an auto-sampler.

Acid properties of the different samples were determined by using pyridine as a probe molecule. Pyridine adsorption was followed by Diffuse reflectance infrared Fourier transform spectroscopy (DRIFTS), which were carried out on a Fourier-transform infrared spectroscopy (FTIR) instrument (Perkin Elmer Frontier) equipped with an environmental chamber (Harrick HVC-DRM). A resolution of 4 cm^{-1} was used with 125 scans averaged to obtain a spectrum from 4000 to 400 cm^{-1}. Prior to each experiment, pyridine adsorption was carried out at 100 °C for 45 min allowing the saturation of the catalyst surface. The physically adsorbed pyridine was then removed from the surface with an air flow (50 mL·min^{-1}). Finally, the IR spectra were recorded at 100 °C. Bands at 1448 and 1537 cm^{-1} (corresponding to Lewis and Brönsted acid sites, respectively) were integrated and acidity was determined using the corresponding molar extinction coefficients.

3 Results and discussion

3.1 Catalysts characterization

First of all, the physicochemical properties of the materials proposed in this study were characterized by XRD and microscopy techniques (SEM and HRTEM). Fig. 1a shows the XRD patterns for Anatase, Rutile and P25, while Fig. 1b shows the patterns for the as-prepared WO_3 catalyst, together with the commercial DTW5 (5 % WO_3 on TiO_2). As expected, pure Anatase and Rutile samples only exhibit corresponding pure crystalline phases (PDF #89-4921 and #77-0440, respectively). In addition, P25, well known as a very efficient heterojunction of anatase

and rutile for a wide variety of photocatalytic processes, exhibits diffraction peaks corresponding to both crystalline phases.

Figure 1

Fig.1 b indicates that the as-prepared WO_3 catalyst exhibits a rather amorphous behavior, although a well-defined peak at $2\theta = 23.1°$ could be identified, which belongs to the (001) phase of a monoclinic structure of WO_3 (PDF #72-0677) [36]. Its low crystallinity (48.6 %, Table 1) compared to the commercial catalytic materials (80 – 85 %, Table 1) could be attributed to the hydrothermal synthesis method, which was performed at low temperature (180 $°C$) without any additional calcination step. For comparison purposes, a similar WO_3 material was calcined at 450 $°C$ in air (1 h, 5 $°C$ min^{-1} heating rate), and the XRD patterns are shown in Fig. S1. After the calcination step, the material evolved to a highly crystalline monoclinic catalyst. Finally, regarding the DTW5 sample, the titanium oxide phase belongs to anatase, and no peaks related to any WO_3 crystalline phase could be identified by XRD. In principle, this could be attributed to a very high dispersion of small WO_3 nanoparticles on the TiO_2 (anatase) support, and/or to a very low crystallinity of WO_3 compared to TiO_2. All materials present a similar crystallite size in the range of 16-23 nm (Table 1).

In order to get more insights into the structural parameters of these catalysts, they were further characterized by HRTEM.

Figure 2

Fig. 2 reveals sharp and clear lattice fringes for all the materials, regardless the crystallinity level. The lattice spacing of Anatase and Rutile are 0.367 nm and 0.249 nm, respectively, in good agreement with theoretical values of (101) plane of the anatase phase [37] and of (101) plane of the rutile phase [38]. It is worth noting that for the commercial DTW5 sample, although there are no significant peaks of WO_3 in the XRD pattern, the lattice spacing of 0.388 nm was found, corresponding to the (001) plane of WO_3 [39]. This clearly revealed the

existence of well dispersed WO_3 with the size of ~14 nm on the TiO_2 (anatase) matrix. Finally, the as-prepared WO_3 synthesized using WCl_6 as the precursor possesses a similar lattice spacing of 0.381 nm, which matches well with the (001) plane of the monoclinic WO_3 previously reported with a similar precursor. [39] In addition, the overall morphology of the catalyst grains was observed by SEM. As shown in Fig. S2, it was found that anatase, P25, DTW5 and WO_3 presented spherical shapes while rutile shows rods-like shape agglomerates.

N_2 adsorption-desorption was carried out to determine the specific surface area (S_{BET}, Table 1) together with the pore size and the porous volume of each material. These parameters could eventually affect their performance for glycerol conversion, owing to the fact that the catalyst active sites along with the adsorption of glycerol as well as its oxidation products usually positively relate to the specific surface area. As shown in Fig. S3, type IV isotherms were obtained with a small hysteresis loop at a relative pressure of 0.7–1.00. Therefore, all materials exhibit, as expected, a mesoporous structure with pore-sizes between 10-15 nm (Table 1). In addition, while Anatase, Rutile and DTW5 showed the highest S_{BET} ($78 – 92$ m^2 g^{-1}), this value was slightly lower for P25 (63 m^2 g^{-1}) and drastically decreased for the as-prepared WO_3 (33 m^2 g^{-1}).

All in all, it seems that in general, the commercial materials exhibit a more crystallized structure with higher specific surface areas compared to the as-prepared WO_3 catalyst. Therefore, in principle, a lower overall catalytic performance could be expected for the latter to a certain extent. Nevertheless, other important features, such as their electronic properties (band gap, charges separation), and concentration of acid sites are known to play a key role in the performance of such photocatalytic materials.

The electronic properties of these materials were first investigated by diffuse reflectance spectroscopy (DRS) in the UV-Vis range. The obtained spectra of samples are shown in Fig. 3a. Comparing Anatase and Rutile samples, a slightly higher adsorption towards the visible

range could be observed for the latter, as previously reported [40]. In addition, as expected, it was found that all the samples could absorb UV light while the as-prepared WO_3 could response to not only UV light but also partially to visible light.

Figure 3

Fig. 3b shows the Tauc plots for band gap calculations using the Kubelka–Munk equation. Briefly, an extrapolation of the linear part of the curve $(\alpha \cdot h\nu)^{1/2}$ (where α is the absorption coefficient) as a function of $h\nu$ defines the band gap energy of the samples considered as indirect band gap semiconductors [41]. As previously mentioned, all the commercial TiO_2-based materials exhibit a band gap compatible with the use of UVA light (> 3.0 eV). Anatase and DTW5 showed an almost identical band gap value, which seems to indicate that the addition of 5 % WO_3 on TiO_2 (anatase) does not significantly affect its electronic properties. In addition, P25, with a anatase/rutile heterojunction, exhibited a slightly smaller band gap, closer to that of rutile. Finally, for the as-prepared WO_3 catalyst, its band gap was 2.61 eV, in good agreement with previous studies, which indicates that its response range to photoirradiation could be expanded to visible light [22]. According to these results, we chose UV light to compare the performance of glycerol photocatalytic oxidation as all catalysts respond to UV light.

In a new effort to characterize the electronic properties of the materials, photocurrent experiments were performed. These tests were carried out in the photoelectrochemical cell described in the experimental section, in neutral media (0.5 M Na_2SO_4 liquid electrolyte, in order to avoid any potential degradation of the materials in acid or alkaline media), upon the application of a constant potential of 0.9 V vs Ag/AgCl reference electrode. All materials were subjected to UV irradiation in step changes of 30 seconds. As shown in Fig. 4, the photocurrent intensity obtained upon irradiation follows this rank: P25＞Anatase≈Rutile≈DTW5＞WO_3.

These results seem to indicate that a better separation rate of photo-generated charges (electrons and holes) [42], [43] upon irradiation could be expected on TiO_2-based materials.

Figure 4

Therefore, the addition of WO_3 seemed to have a detrimental effect on such phenomenon. If the separation of these photo-generated charges is related to the overall activity of oxidation on these materials, we could expect a higher glycerol photo-oxidation rate on TiO_2 than on WO_3-based catalysts.

Finally, the nature and relative amount of acid sites of P25, DTW5 and WO_3 were characterized by adsorption of pyridine followed by diffuse reflection infrared spectroscopy (DRIFT).

Figure 5

Figure 5 depicts the spectra of pyridine chemisorbed at 100 °C. The bands obtained at 1448 and 1542 cm^{-1} could be attributed to Lewis acid sites and to protonated pyridine molecules bound to surface Brönsted acid sites, respectively [44], [45]. In addition, Table 2 presents the calculated quantitative values of both acid sites, the overall amount and the ratio between them. If we compare the results for P25 (TiO_2) and WO_3, it can be clearly observed that WO_3 possesses the highest percentage of Brönsted and total acid sites. This is expected considering that tungsten-based catalysts are well-known for their acidic properties. For instance, Ganji et al. [46] reported an overall higher acidity of WO_3 and WO_3/TiO_2 materials compared to TiO_2, obtained by both pyridine-FTIR and NH_3-TPD (temperature programmed desorption). That could explain that the DTW5, compared with P25, also exhibited a higher amount of Brönsted and total acid sites. These acidic properties are expected to play a very important role in the photocatalytic activity of these materials towards glycerol activation. For instance, $Pt/WO_3/Al_2O_3$ catalysts have been reported as one of the most successful catalytic systems for the effective conversion of glycerol to 1,3-propanediol by thermal-hydrogenolysis [47], where Brønsted acid sites are considered to play a key role for the adsorption/activation of the

secondary C-O bond in glycerol [48]. Also, in a previous study by Checa et al. dealing with the same reaction [44] it was found that the addition of tungsten to a Pt/ZrO$_2$ catalyst enhanced its selective performance of the target product 1,3-propanediol, most likely due to the creation of a higher concentration of Brönsted acid sites.

To summarize this section, the characterization results exhibit overall enhanced physicochemical properties of TiO$_2$-based materials compared to WO$_3$ catalysts in terms of specific surface area, crystallinity, and photo-generated charge separation. However, the WO$_3$ –based materials are much more acidic, containing a higher amount of Brönsted acid sites.

3.2 Photocatalytic activity

All the catalysts previously characterized were tested for photocatalytic oxidation of glycerol. Figure 6 shows the evolution of the glycerol conversion with time upon irradiation. Regarding all the TiO$_2$-based materials, a significant oxidation of glycerol was achieved after 5 hours (Fig. 6a). However, for the as-prepared WO$_3$ catalyst, the glycerol consumption rate is lower, and therefore the reaction time was extended up to 22 h (Fig. 6b). In order to prove that the activity was due to the photocatalysis, blank experiments over P25, DTW5 and WO$_3$ (in the dark, Fig. S4a-c) and a direct photolysis of glycerol (without any catalyst in the light, Fig. S4d) were performed, where the glycerol conversion was negligible.

Figure 6

As observed in Fig. 6a, P25 seemed to be the most active material, achieving a complete glycerol conversion after 4 h. Therefore, the photocatalytic activity obtained upon irradiation for glycerol oxidation obeys the order P25＞Anatase＞Rutile>DTW5＞WO$_3$. With regards to P25, its outstanding activity has been already proven for a wide variety of photocatalytic processes, including glycerol photooxidation [24], [27], [28]. P25 consists of a mixed phase of anatase and rutile in a ratio of about 4:1. In the so-called anatase/rutile heterojunctions, upon UV irradiation, the photogenerated electrons from anatase phase are transferred to the rutile

phase on account of its lower conduction band energy [49]. This results in a more efficient separation of the photogenerated charge carriers, as observed in the photocurrent experiments (Fig. 4). Another evidence of the creation of this heterojunction was observed in the DRS experiments, where the band gap for P25 was in-between that of anatase and rutile (Fig. 3b). One may expect a similar behavior for the DTW5 material. As a matter of fact, WO_3/TiO_2 composites have been previously developed and reported to enhance the separation of photogenerated charge carriers on the heterojunctions between both phases together with a modification of the band gap of TiO_2 towards a more visible-light range [50]. However, in this case we could not observe a significant heterojunction, since the band gap for DTW5 was found to be almost identical to that of anatase (Fig. 3b). Furthermore, the photocurrent obtained for DTW5 was even slightly lower than that for Anatase (Fig. 4). Therefore, we conclude that the low loading of WO_3 (5 %) on anatase can neither enhance the separation of charge carriers nor the conversion of glycerol. It is worth noting therefore that the photocurrent activity observed in Fig. 4 obeys the same order than the overall glycerol conversion activity after 5 h of irradiation observed in Fig. 6. This suggests that the photocatalytic degradation of glycerol is strongly related with the separation of the electrons and holes produced upon irradiation.

The aim of this study is to enhance the production of added-value products by photocatalytic oxidation of glycerol. Fig. 7 shows the products distribution with time for all the materials.

Figure 7

The main oxidation products observed were glyceraldehyde, DHA, glycolic acid, tartronic acid, oxalic acid, formic acid and acetic acid. Nevertheless, the amount and distribution of each of these products is highly influenced by the nature of the photocatalytic material. Starting with the most active material, P25, we can clearly observe that some of the main oxidation products, including glyceraldehyde, DHA and formic acid are produced during a short period of around 1 h. A similar effect was observed in the Anatase catalyst, although the products distribution

and amount were different, as expected in view of the observed lower overall conversion (Fig. 6). On the other hand, the Rutile catalyst seemed to produce a significant amount of formic acid.

Our results for both, P25 and Anatase photocatalysts are in good agreement with the model proposed by Jedsukontorn et al. [51], [52] for glycerol conversion on TiO_2 (anatase). According to those studies, upon UV irradiation, glycerol acts as a hole scavenger of the photogenerated holes [51], or reacts with the reactive oxidizing species [52], oxidizing it to both glyceraldehyde and DHA. Minero et al. [28] also proposed that the formation of these species could be mediated by ˙OH radicals. Glyceraldehyde is produced when the primary –OH group is adsorbed and oxidized, while DHA is produced upon the oxidation of the secondary –OH group of glycerol. The glyceraldehyde could be then oxidized to produce glyceric acid, while the DHA could be rearranged into glyceraldehyde [51]. It could be expected afterwards that the products keep evolving into smaller organic molecules, such as tartronic acid, oxalic acid, and as observed in this study, formic acid. These reaction routes are in good agreement with the results obtained for Anatase and P25, since the observed reaction products evolved with time and then disappeared.

However, for Rutile, the main product seemed to be formic acid, and we could not observe a similar evolution for the other TiO_2 catalysts. In this sense, Augugliaro et al. [27] proposed a mechanism where all the species are produced in parallel on P25, anatase and rutile catalysts, including glyceraldehyde, DHA, formic acid and CO_2. Minero et al. [28] also suggested a model where C2 + C1 products could also be produced in parallel by direct electron transfer (in this case over P25). We believe that these mechanisms are in good agreement with the results obtained for Rutile, where the formation of formic acid seemed to be the product of a parallel process.

The most interesting results were obtained with the WO_3-based materials. Starting with the as-prepared WO_3, a completely different behavior was observed. In this case, as opposed to Anatase and P25, the concentration of reaction products gradually increased with time. The main product was glyceraldehyde, followed by DHA and then by smaller quantities of further oxidized products. These results suggest a similar first oxidation step as previously explained for TiO_2, where glycerol undergoes a first oxidation towards glyceraldehyde and DHA. Considering that the former is the result of the oxidation of primary (terminal) –OH groups of glycerol and that we have two primary -OH groups its likelihood to be produced is much higher compared to that for the production of DHA, which is the result of the oxidation of the secondary –OH group in glycerol. Moreover, on the one hand, in presence of WO_3, the ratio glyceraldehyde/DHA is higher than 2. It suggests that in the presence of WO_3, a fraction of the DHA formed is probably converted into glyceraldehyde and on the other hand, these high added-value products seemed to desorb in the liquid phase, rather than to undergo a further oxidation towards smaller molecules. These photocatalytic properties are of paramount importance for the development of novel catalysts with high selectivity towards glyceraldehyde. However, as discussed in Fig. 6, the photocatalytic reaction on this material is rather slow compared to that of Anatase, Rutile and P25, and longer reaction times were required with this system for practical purposes.

Before discussing the photocatalytic behavior of the DTW5 material, two parameters will be introduced to compare the performance of pure TiO_2-based materials (Anatase, Rutile and P25) and the as-prepared WO_3. Fig. 8 shows the variation of the products selectivity while Fig. 9 shows the variation of the products yield, both of them as a function of the glycerol conversion.

Figure 8

Figure 9

These figures allow us to compare the production of the added-value products of interest (in this case glyceraldehyde) at glycerol isoconversion conditions. As expected for P25 and Anatase according to the results discussed in Fig. 7, high selectivities and yields to oxidation products are only achieved at low conversion levels. Unfortunately, there was only one products analysis below 40% of conversion due to the fast kinetics on P25. As the system evolved in time, the conversion increased but the production of valuable products decreased. In addition, since the sum of all the liquid products selectivity is far from 100 % at all the conversion levels, it could be assumed that CO_2 could be also produced. This hypothesis is confirmed considering the TOC measured after about 45% of conversion (Fig. 10).

Figure 10

This was also the case for the Rutile catalyst which predominantly produces formic acid. Therefore, none of the pure TiO_2-based catalysts exhibited a significant performance towards the production of glyceraldehyde.

Nevertheless, in these figures we could clearly observe that the as-prepared WO_3 catalyst exhibited an outstanding activity towards the production of the desired product, glyceraldehyde, even under high conversion levels. As a matter of fact, with a relatively constant selectivity towards this product, its yield gradually increased with the overall glycerol conversion. In addition, the overall selectivity of liquid organic products over this catalyst is much higher than that of the TiO_2 materials, which indicates that the total glycerol oxidation towards CO_2 is much more unlikely as confirmed by TOC analysis (Fig. 10). Besides, WO_3 post-treated via calcination at 450 ºC exhibited a slightly superior glycerol conversion owing to its higher crystallinity (Fig. S1), with similar values of glyceraldehyde selectivity and yield (Fig. S5). Therefore, TiO_2-based materials (mainly Anatase and P25) exhibited, as expected, a great overall catalytic performance for the oxidation of glycerol, but a rather poor selectivity to glyceraldehyde, while the as-prepared (and calcined) WO_3 catalysts exhibited an interesting

selectivity/yield towards this product, even under high conversion levels. The main issue of this material is related to the rather slow kinetics, which could lower the added-value of this material for practical purposes.

In order to overcome this issue, the DTW5 catalyst was tested for the photocatalytic oxidation of glycerol. In Figs. 7-9 we can clearly observe that the presence of a small amount of WO_3 (5 %) in the anatase support led to a completely different behavior in the desired direction. Hence, as opposed to the Anatase photocatalyst, the reaction products formed on DTW5 did not seem to disappear with time, but rather to increase in a similar way to that obtained with the as-prepared WO_3 material. In addition, the selectivity/yield towards glyceraldehyde was much higher for DTW5 compared to the TiO_2 catalysts. Table 3 shows the values for glyceraldehyde selectivity and yield at similar glycerol conversion values (43-47 %) over all the photocatalysts. While both parameters are rather low for TiO_2 materials in our study (< 5 %) and for other noble metal-free TiO_2-based photocatalysts in publications [27], [28], [53], [54], glyceraldehyde yields/selectivities of 13 %/29 % and 8 %/19 % were obtained for the as-prepared WO_3 and for DTW5, respectively.

In addition, total organic carbon analysis (TOC) of the liquid solutions were performed for the different photocatalytic systems when the glycerol conversion achieved a value ~ 45 %. The obtained values were compared with initial concentration of glycerol (Fig. 10). The results obtained allowed us to confirm the level of mineralization of glycerol over the different catalysts upon irradiation. In addition, as we discussed in the previous figures, the modification of anatase with WO_3 (DTW5) allowed to avoid the mineralization compared to the Anatase catalyst, in good agreement with the higher selectivity exhibited by this material towards liquid added-value products, mainly glyceraldehyde.

Therefore, the photocatalytic activity results obtained in this study clearly demonstrated, for the first time in literature, an outstanding performance of WO_3-based materials for the selective

photocatalytic oxidation of glycerol to glyceraldehyde. In particular, the commercial 5 % WO_3/TiO_2 (anatase) catalyst allows to combine the main features of anatase (fast kinetics for glycerol conversion) and WO_3 (high selectivity towards glyceraldehyde). These results are in good agreement with the characterization study described in section 3.1. The textural parameters (crystallinity, crystal size and specific surface area, Table 1) for Anatase, Rutile, P25 and DTW5 were relatively similar and cannot explain the differences observed in photocatalytic properties. Nevertheless, the overall activity for glycerol conversion was strongly correlated with the electronic properties of these materials, namely the separation of photogenerated charge carriers (as observed by the photocurrent characterization tests, Fig. 4). This phenomenon was previously observed in many photocatalytic processes, since an enhanced separation of e^- and holes is indeed one of the most common strategies to improve the overall performance of the photocatalytic system. This is usually managed either by doping the semiconductor catalyst with a metal (e^- trap), or by the formation of heterojunctions between different materials or different phases of the same material [49].

However, the enhanced glyceraldehyde selectivity observed for DTW5 catalyst compared to Anatase (or any other TiO_2-based catalyst) could not be explained by its electronic properties. Considering that both materials exhibit an almost identical band gap (Fig. 3b), and the fact that DTW5 shows lower photocurrent activity (i.e., worse separation of photogenerated carriers, Fig. 4), the formation of a successful heterojunction between TiO_2 and WO_3 could be disregarded. We believe therefore that the outstanding performance of DTW5 towards glyceraldehyde production could be attributed to its enhanced surface acidity.

In this sense, previous studies dealing with the thermal catalytic hydrogenolysis of glycerol already proved that WO_3 plays a role of paramount importance due to the presence of Bronsted sites, which allow for the selective activation of C-O bonds in glycerol [47]. Furthermore, the obtained results could be correlated with a previous study by Lopez-Tenllado et al.[55] dealing

with the selective photooxidation of organic molecules (crotyl alcohol to crotonaldehyde). This reaction was performed on titania, ceria and bismuth tungstate catalysts, where the latter was the most selective. This phenomenon was attributed to the lowest adsorption of the aldehyde reaction product on the tungsten-based catalyst. In other words, this material seemed to favor the desorption of the desired product, avoiding its further photooxidation. Therefore, according to the obtained results and the above-mentioned studies, we suggest that the higher selectivity/yield achieved by the WO_3-based catalysts can be attributed to the incorporation of additional acid sites to the anatase semiconductor. These new sites would allow to enhance the selective activation of primary C-O bonds in glycerol towards the production of glyceraldehyde and, on the other hand, to quickly desorb aldehyde products in the liquid phase.

All in all, this study demonstrates that WO_3-based materials are active for the valorization of glycerol towards a high added-value product: glyceraldehyde. All these materials exhibit outstanding advantages. On the one hand, the as-prepared WO_3 catalyst leads to a high yield of glyceraldehyde even at very high conversion levels. However, its applicability could be compromised by its slow overall kinetics. In this sense, the calcined WO_3 catalyst, with improved crystallinity, seemed to enhance the kinetics without compromising the glyceraldehyde yield, although the calcination step could eventually increase the overall production cost of this material. Finally, commercial DTW5 led to lower glyceraldehyde yields than pure WO_3 catalysts (but still much higher than those for pure TiO_2-based materials), and overall faster kinetics. Therefore, further studies could optimize the composition and synthesis procedure of the photocatalyst for practical purposes.

4 Conclusions

In this study we demonstrated, for the first time in literature, the high performance of WO_3-based catalysts for the selective photooxidation of glycerol towards glyceraldehyde. By

comparing the activity of pure TiO$_2$ (Anatase, Rutile and P25$_{\text{anatase/rutile}}$) and pure WO$_3$ (prepared by a simple hydrothermal method), we can conclude that: i) TiO$_2$ catalysts allowed for a higher overall conversion of glycerol, where the selectivity to glyceraldehyde was hindered by its further photooxidation, and ii) WO$_3$ catalysts exhibit slower kinetics for glycerol oxidation, but show an outstanding selectivity and yield of glyceraldehyde. While the activity of TiO$_2$ was attributed to electronic effects (better separation of photogenerated charge carriers), the high glyceraldehyde selectivity of WO$_3$ was linked to its enhanced acidity, that selectively activate C-O bonds in glycerol, and facilitate the desorption of glyceraldehyde (avoiding its further photooxidation). Hence, a commercial WO$_3$/TiO$_2$ material (DTW5) was proven to combine the best features of both semiconductors, with high levels of glycerol conversion and selectivity to glyceraldehyde. This study opens therefore a new field dealing with the development of advanced photocatalytic materials for an advanced valorization of glycerol into high added-value products.

Acknowledgement

References

[1] OECD/FAO, OECD-FAO Agricultural Outlook 2016-2025. OECD Publishing, Paris, (2016).

[2] O.P. Paris/FAO, OECD-FAO Agricultural Outlook 2020-2029, 2020.

[3] C. Santibáñez, M.T. Varnero, M. Bustamante, Residual glycerol from biodiesel manufacturing, waste or potential source of bioenergy: a review, Chil. J. Agric. Res. 71 (2011) 469–475.

[4] M. Pagliaro, R. Ciriminna, H. Kimura, M. Rossi, C. Della Pina, From glycerol to value-added products, Angew. Chemie - Int. Ed. 46 (2007) 4434–4440. https://doi.org/10.1002/anie.200604694.

[5] Y. Kwon, M.T.M. Koper, Combining voltammetry with HPLC: Application to electro-oxidation of glycerol, Anal. Chem. 82 (2010) 5420–5424. https://doi.org/10.1021/ac101058t.

[6] E. Diguilio, E.D. Galarza, M.E. Domine, L.B. Pierella, M.S. Renzini, Tuning product selectivity in the catalytic oxidation of glycerol by employing metal-ZSM-11 materials, New J. Chem. 44 (2020) 4363–4375.

[7] P.M. Walgode, R.P. V Faria, A.E. Rodrigues, A review of aerobic glycerol oxidation processes using heterogeneous catalysts: a sustainable pathway for the production of dihydroxyacetone, Catal. Rev. (2020) 1–90.

[8] C. Detoni, A.R.P. da Silva, M.M.V.M. Souza, Effect of Pt/HZSM-5 dealumination by high temperature reduction on glycerol oxidation, J. Porous Mater. (2020) 1–11.

[9] D.E. Castillo, J.E. Keri, Chemical peels in the treatment of acne: patient selection and perspectives, Clin. Cosmet. Investig. Dermatol. 11 (2018) 365.

[10] L.C.D. Coelho, M.L. Nelson Filho, R.P. V Faria, A.F.P. Ferreira, A.M. Ribeiro, A.E. Rodrigues, Separation of tartronic and glyceric acids by simulated moving bed chromatography, J. Chromatogr. A. 1563 (2018) 62–70.

[11] A. Mendoza, R. Romero, G.P. Gutiérrez-Cedillo, G. López-Tellez, O. Lorenzo-González, R.M. Gómez-Espinosa, R. Natividad, Selective production of dihydroxyacetone and glyceraldehyde by photo-assisted oxidation of glycerol, Catal. Today. 358 (2020) 149–154.

[12] A. Behr, J. Eilting, K. Irawadi, J. Leschinski, F. Lindner, Improved utilisation of renewable resources: New important derivatives of glycerol, Green Chem. 10 (2008) 13–30.

[13] D. Liang, J. Gao, H. Sun, P. Chen, Z. Hou, X. Zheng, Selective oxidation of glycerol

with oxygen in a base-free aqueous solution over MWNTs supported Pt catalysts, Appl. Catal. B Environ. 106 (2011) 423–432. https://doi.org/10.1016/j.apcatb.2011.05.050.

[14] H. Kimura, K. Tsuto, T. Wakisaka, Y. Kazumi, Y. Inaya, Selective oxidation of glycerol on a platinum-bismuth catalyst, Appl. Catal. A, Gen. 96 (1993) 217–228. https://doi.org/10.1016/0926-860X(90)80011-3.

[15] H. Tan, C. Yao, T. Zhan, W. Li, J. Zhu, G. Wang, W. Liu, M. Sun, S. Wang, Selective oxidation of glycerol to dihydroxyacetone over N-doped porous carbon stabilized CuxO supported Au catalysts, Mol. Catal. 498 (2020) 111243. https://doi.org/10.1016/j.mcat.2020.111243.

[16] A. Mendoza, R. Romero, G.P. Gutiérrez-Cedillo, G. López-Tellez, O. Lorenzo-González, R.M. Gómez-Espinosa, R. Natividad, Selective production of dihydroxyacetone and glyceraldehyde by photo-assisted oxidation of glycerol, Catal. Today. (2020) 0–1. https://doi.org/10.1016/j.cattod.2019.09.035.

[17] J. Payormhorm, R. Idem, Synthesis of C-doped TiO_2 by sol-microwave method for photocatalytic conversion of glycerol to value-added chemicals under visible light, Appl. Catal. A Gen. 590 (2020) 117362. https://doi.org/10.1016/j.apcata.2019.117362.

[18] A.L. Imbault, R. Farnood, Selective oxidation of crude glycerol to dihydroxyacetone in a biphasic photoreactor, Catalysts. 10 (2020). https://doi.org/10.3390/catal10040360.

[19] Z. Zhang, L. Xin, W. Li, Electrocatalytic oxidation of glycerol on Pt/C in anion-exchange membrane fuel cell: Cogeneration of electricity and valuable chemicals, Appl. Catal. B Environ. 119–120 (2012) 40–48. https://doi.org/10.1016/j.apcatb.2012.02.009.

[20] C. Liu, M. Hirohara, T. Maekawa, R. Chang, T. Hayashi, C.Y. Chiang, Selective electro-oxidation of glycerol to dihydroxyacetone by a non-precious electrocatalyst – CuO, Appl. Catal. B Environ. 265 (2020) 118543. https://doi.org/10.1016/j.apcatb.2019.118543.

[21] D. Lee, Y. Kim, H. Han, W.B. Kim, H. Chang, T.M. Chung, J.H. Han, H.W. Kim, H.J. Kim, Atomic-layer-deposited SnO_2 on Pt/C prevents sintering of Pt nanoparticles and affects the reaction chemistry for the electrocatalytic glycerol oxidation reaction, J. Mater. Chem. A. 8 (2020) 15992–16005. https://doi.org/10.1039/d0ta02509g.

[22] D. Raptis, V. Dracopoulos, P. Lianos, Renewable energy production by photoelectrochemical oxidation of organic wastes using WO_3 photoanodes, J. Hazard. Mater. 333 (2017) 259–264. https://doi.org/https://doi.org/10.1016/j.jhazmat.2017.03.044.

[23] B. Qiu, M. Xing, J. Zhang, Recent advances in three-dimensional graphene based

materials for catalysis applications, Chem. Soc. Rev. 47 (2018) 2165–2216. https://doi.org/10.1039/c7cs00904f.

[24] V. Maurino, A. Bedini, M. Minella, F. Rubertelli, E. Pelizzetti, C. Minero, Glycerol transformation through photocatalysis: A possible route to value added chemicals, J. Adv. Oxid. Technol. 11 (2008) 184–192.

[25] P. Panagiotopoulou, E.E. Karamerou, D.I. Kondarides, Kinetics and mechanism of glycerol photo-oxidation and photo-reforming reactions in aqueous TiO_2 and Pt/TiO_2 suspensions, Catal. Today. 209 (2013) 91–98. https://doi.org/10.1016/j.cattod.2012.09.029.

[26] M. de Oliveira Melo, L.A. Silva, Visible light-induced hydrogen production from glycerol aqueous solution on hybrid Pt--CdS--TiO_2 photocatalysts, J. Photochem. Photobiol. A Chem. 226 (2011) 36–41.

[27] V. Augugliaro, H.A.H. El Nazer, V. Loddo, A. Mele, G. Palmisano, L. Palmisano, S. Yurdakal, Partial photocatalytic oxidation of glycerol in TiO_2 water suspensions, Catal. Today. 151 (2010) 21–28. https://doi.org/10.1016/j.cattod.2010.01.022.

[28] C. Minero, A. Bedini, V. Maurino, Glycerol as a probe molecule to uncover oxidation mechanism in photocatalysis, Appl. Catal. B Environ. 128 (2012) 135–143. https://doi.org/10.1016/j.apcatb.2012.02.014.

[29] I.M. Szilágyi, E. Santala, M. Heikkilä, V. Pore, M. Kemell, T. Nikitin, G. Teucher, T. Firkala, L. Khriachtchev, M. Räsänen, M. Ritala, M. Leskelä, Photocatalytic properties of WO_3/TiO_2 core/shell nanofibers prepared by electrospinning and atomic layer deposition, Chem. Vap. Depos. 19 (2013) 149–155. https://doi.org/10.1002/cvde.201207037.

[30] I.M. Szilágyi, B. Fórizs, O. Rosseler, Á. Szegedi, P. Németh, P. Király, G. Tárkányi, B. Vajna, K. Varga-Josepovits, K. László, A.L. Tóth, P. Baranyai, M. Leskelä, WO_3 photocatalysts: Influence of structure and composition, J. Catal. 294 (2012) 119–127. https://doi.org/10.1016/j.jcat.2012.07.013.

[31] M. Tahir, M. Siraj, B. Tahir, M. Umer, H. Alias, N. Othman, Au-NPs embedded Z--scheme WO_3/TiO_2 nanocomposite for plasmon-assisted photocatalytic glycerol-water reforming towards enhanced H2 evolution, Appl. Surf. Sci. 503 (2020) 144344.

[32] M. Stelmachowski, M. Marchwicka, E. Grabowska, M. Diak, The photocatalytic conversion of (biodiesel derived) glycerol to hydrogen-A short review and preliminary experimental results part 1: A review, J. Adv. Oxid. Technol. 17 (2014) 167–178.

[33] X. Liu, H. Zhai, P. Wang, Q. Zhang, Z. Wang, Y. Liu, Y. Dai, B. Huang, X. Qin, X.

Zhang, Synthesis of a WO_3 photocatalyst with high photocatalytic activity and stability using synergetic internal Fe^{3+} doping and superficial Pt loading for ethylene degradation under visible-light irradiation, Catal. Sci. Technol. 9 (2019) 652–658.

[34] C.M. Hung, N. Van Duy, V. Van Quang, N. Van Toan, N. Van Hieu, N.D. Hoa, others, Facile synthesis of ultrafine rGO/WO_3 nanowire nanocomposites for highly sensitive toxic NH3 gas sensors, Mater. Res. Bull. 125 (2020) 110810.

[35] Z. Chen, Y. Peng, F. Liu, Z. Le, J. Zhu, G. Shen, D. Zhang, M. Wen, S. Xiao, C.-P. Liu, others, Hierarchical nanostructured WO3 with biomimetic proton channels and mixed ionic-electronic conductivity for electrochemical energy storage, Nano Lett. 15 (2015) 6802–6808.

[36] M.S. Koo, X. Chen, K. Cho, T. An, W. Choi, In Situ Photoelectrochemical Chloride Activation Using a WO_3 Electrode for Oxidative Treatment with Simultaneous H_2 Evolution under Visible Light, Environ. Sci. Technol. 53 (2019) 9926–9936. https://doi.org/10.1021/acs.est.9b02401.

[37] Y. Ren, L.J. Hardwick, P.G. Bruce, Lithium Intercalation into Mesoporous Anatase with an Ordered 3D Pore Structure, Angew. Chemie. 122 (2010) 2624–2628. https://doi.org/10.1002/ange.200907099.

[38] L. Miao, P. Jin, K. Kaneko, A. Terai, N. Nabatova-Gabain, S. Tanemura, Preparation and characterization of polycrystalline anatase and rutile TiO_2 thin films by rf magnetron sputtering, Appl. Surf. Sci. 212–213 (2003) 255–263. https://doi.org/10.1016/S0169-4332(03)00106-5.

[39] S. Pokhrel, J. Birkenstock, M. Schowalter, A. Rosenauer, L. Mädler, Growth of ultrafine single crystalline WO_3 nanoparticles using flame spray pyrolysis, Cryst. Growth Des. 10 (2010) 632–639. https://doi.org/10.1021/cg9010423.

[40] L. Elsellami, F. Dappozze, N. Fessi, A. Houas, C. Guillard, Highly photocatalytic activity of nanocrystalline TiO_2 (anatase, rutile) powders prepared from $TiCl_4$ by sol–gel method in aqueous solutions., Process Saf. Environ. Prot. 113 (2018) 109–121. https://doi.org/10.1016/j.psep.2017.09.006.

[41] N. Fessi, M.F. Nsib, L. Cardenas, C. Guillard, F. Dappozze, A. Houas, F. Parrino, L. Palmisano, G. Ledoux, D. Amans, Y. Chevalier, Surface and Electronic Features of Fluorinated TiO_2 and Their Influence on the Photocatalytic Degradation of 1-Methylnaphthalene, J. Phys. Chem. C. 124 (2020) 11456–11468. https://doi.org/10.1021/acs.jpcc.0c01929.

[42] S. Wu, X. Tan, J. Lei, H. Chen, L. Wang, J. Zhang, Ga-Doped and Pt-Loaded Porous

TiO$_2$-SiO$_2$ for Photocatalytic Nonoxidative Coupling of Methane, J. Am. Chem. Soc. 141 (2019) 6592–6600. https://doi.org/10.1021/jacs.8b13858.

[43]   J. Hu, L. Wang, P. Zhang, C. Liang, G. Shao, Construction of solid-state Z-scheme carbon-modified TiO$_2$/WO$_3$ nanofibers with enhanced photocatalytic hydrogen production, J. Power Sources. 328 (2016) 28–36. https://doi.org/10.1016/j.jpowsour.2016.08.001.

[44]   M. Checa, V. Montes, J. Hidalgo-Carrillo, A. Marinas, F.J. Urbano, Influence of Boron, Tungsten and Molybdenum Modifiers on Zirconia Based Pt Catalyst for Glycerol Valorization, Nanomater. . 9 (2019). https://doi.org/10.3390/nano9040509.

[45]   J. González, J.A. Wang, L.F. Chen, M.E. Manríquez, J.M. Dominguez, Structural Defects, Lewis Acidity, and Catalysis Properties of Mesostructured WO$_3$/SBA-15 Nanocatalysts, J. Phys. Chem. C. 121 (2017) 23988–23999. https://doi.org/10.1021/acs.jpcc.7b06373.

[46]   P. Ganji, S. Roy, Trade-off between acidic sites and crystallinity of the WO$_3$-TiO$_2$ catalyst toward dehydration of glucose to 5-hydroxymethylfurfural, Energy and Fuels. 33 (2019) 5293–5303. https://doi.org/10.1021/acs.energyfuels.9b00461.

[47]   T. Kurosaka, H. Maruyama, I. Naribayashi, Y. Sasaki, Production of 1,3-propanediol by hydrogenolysis of glycerol catalyzed by Pt/WO$_3$/ZrO$_2$, Catal. Commun. 9 (2008) 1360–1363. https://doi.org/https://doi.org/10.1016/j.catcom.2007.11.034.

[48]   T. Aihara, H. Miura, T. Shishido, Investigation of the mechanism of the selective hydrogenolysis of CO bonds over a Pt/WO$_3$/Al$_2$O$_3$ catalyst, Catal. Today. 352 (2020) 73–79. https://doi.org/https://doi.org/10.1016/j.cattod.2019.10.008.

[49]   N. Subramanian, A. Caravaca, F.R. García-García, M. Bowker, Sustainable hydrogen and/or syngas production: New approaches to reforming, 2017. https://doi.org/10.1142/9781786341228_0001.

[50]   S. Palmas, P.A. Castresana, L. Mais, A. Vacca, M. Mascia, P.C. Ricci, TiO$_2$–WO$_3$ nanostructured systems for photoelectrochemical applications, RSC Adv. 6 (2016) 101671–101682. https://doi.org/10.1039/C6RA18649A.

[51]   T. Jedsukontorn, V. Meeyoo, N. Saito, M. Hunsom, Route of glycerol conversion and product generation via TiO$_2$-induced photocatalytic oxidation in the presence of H$_2$O$_2$, Chem. Eng. J. 281 (2015) 252–264. https://doi.org/10.1016/j.cej.2015.06.078.

[52]   T. Jedsukontorn, T. Ueno, N. Saito, M. Hunsom, Mechanistic aspect based on the role of reactive oxidizing species (ROS) in macroscopic level on the glycerol photooxidation over defected and defected-free TiO$_2$, J. Photochem. Photobiol. A Chem. 367 (2018)

270–281. https://doi.org/10.1016/j.jphotochem.2018.08.030.

[53] A.L. Imbault, J. Gong, R. Farnood, Photocatalytic production of dihydroxyacetone from glycerol on TiO$_2$ in acetonitrile, RSC Adv. 10 (2020) 4956–4968.

[54] T. Jedsukontorn, T. Ueno, N. Saito, M. Hunsom, Narrowing band gap energy of defective black TiO$_2$ fabricated by solution plasma process and its photocatalytic activity on glycerol transformation, J. Alloys Compd. 757 (2018) 188–199.

[55] F.J. López-Tenllado, S. Murcia-López, D.M. Gómez, A. Marinas, J.M. Marinas, F.J. Urbano, J.A. Nav\'\io, M.C. Hidalgo, J.M. Gatica, A comparative study of Bi$_2$WO$_6$, CeO$_2$, and TiO$_2$ as catalysts for selective photo-oxidation of alcohols to carbonyl compounds, Appl. Catal. A Gen. 505 (2015) 375–381.

Figure captions

Figure 1. X-ray diffraction (XRD) patterns of commercial catalysts (Anatase, Rutile, P25 and DTW5) and as-prepared WO_3

Figure 2. High-resolution transmission electron microscopy (HRTEM) images of Anatase, Rutile, DTW5 and as-prepared WO_3 catalysts

Figure 3. (a) UV-Vis diffuse reflectance spectroscopy (DRS) spectra and (b) Tauc plot for band gap determination for commercial catalysts (Anatase, Rutile, P25 and DTW5) and as-prepared WO_3

Figure 4. Transient photocurrent response for commercial catalysts (Anatase, Rutile, P25 and DTW5) and as-prepared WO_3. Conditions: neutral reaction media (0.5 M Na2SO4), applied potential: 0.9 V vs Ag/AgCl. The experiments were performed in a photoelectrochemical cell, where the catalyst was supported on an ITO glass (working electrode), and a Pt counter electrode was used for polarization purposes.

Figure 5. pyridine-DRIFTS spectra of P25, DTW5 and WO_3. B and L denote Brönsted and Lewis acid sites, respectively.

Figure 6. Glycerol conversion over commercial catalysts (Anatase, Rutile, P25 and DTW5) and as-prepared WO_3. Reaction conditions: Room temperature, Glycerol initial concentration: 1.10 mmol L^{-1}, Volume of glycerol solution: 30 mL, UV irradiation intensity of 5.60 mW cm^2

Figure 7. Evolution of products with time over commercial catalysts (Anatase, Rutile, P25 and DTW5) and as-prepared WO_3. Reaction conditions: Room temperature, Glycerol initial concentration: 1.10 mmol L^{-1}, Volume of glycerol solution: 30 mL, UV irradiation intensity of 5.60 mW cm^{-2}

Figure 8. Variation of products selectivity with respect to the glycerol conversion over commercial catalysts (Anatase, Rutile, P25 and DTW5) and as-prepared WO_3. Reaction conditions: Room temperature, Glycerol initial concentration: 1.10 mmol L^{-1}, Volume of glycerol solution: 30 mL, UV irradiation intensity of 5.60 mW cm^{-2}

Figure 9. Variation of products yield with respect to the glycerol conversion over commercial catalysts (Anatase, Rutile, P25 and DTW5) and as-prepared WO_3. Reaction conditions: Room temperature, Glycerol initial concentration: 1.10 mmol L^{-1}, Volume of glycerol solution: 30 mL, UV irradiation intensity of 5.60 mW cm^{-2}

Figure 10. Total organic carbon (TOC) measurement of the liquid solutions for commercial catalysts (Anatase, Rutile, P25 and DTW5) and as-prepared WO_3, after the achieved glycerol conversion was ~45 %. Reaction conditions: Room temperature, Glycerol initial concentration: 1.10 mmol L^{-1} (TOC: 40.4 ± 2 mg/L), Volume of glycerol solution: 30 mL, UV irradiation intensity of 5.60 mW cm^{-2}

Tables captions:

Table 1. BET specific surface area, pore volume, pore size, crystallinity and average crystallite size of the photocatalysts

Table 2. Comparison of Lewis, Brönsted and total acid sites of P25, DTW5 and WO_3, obtained by pyridine-DRIFTS

Table 3. Comparison of glyceraldehyde Yield and Selectivity for all the photocatalysts at similar levels of glycerol conversion
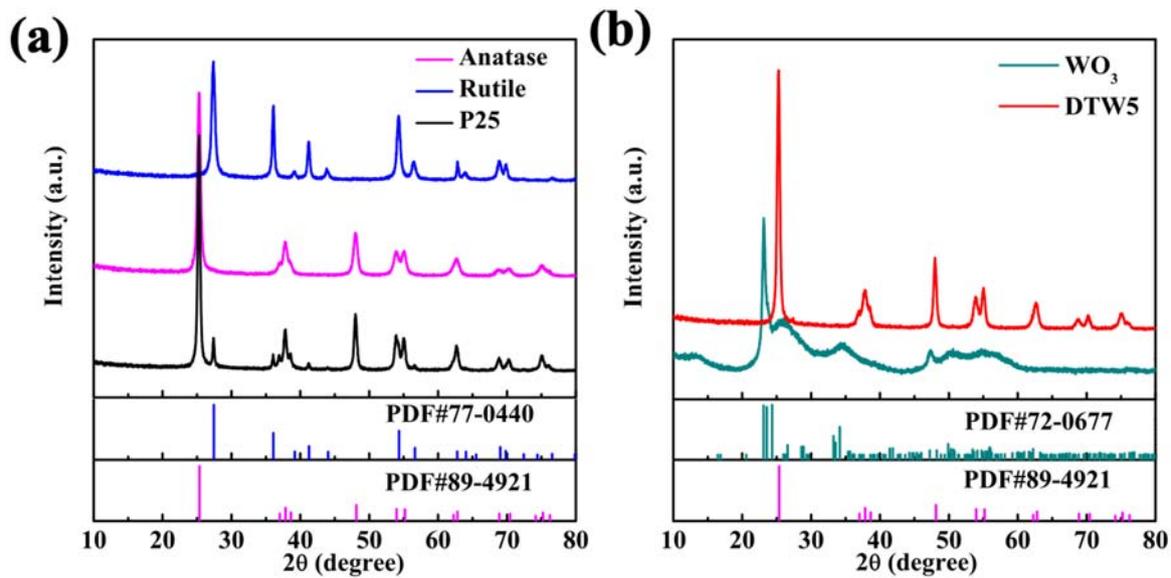
Fig. 1. X-ray diffraction (XRD) patterns of commercial catalysts (Anatase, Rutile, P25 and DTW5) and as-prepared WO_3
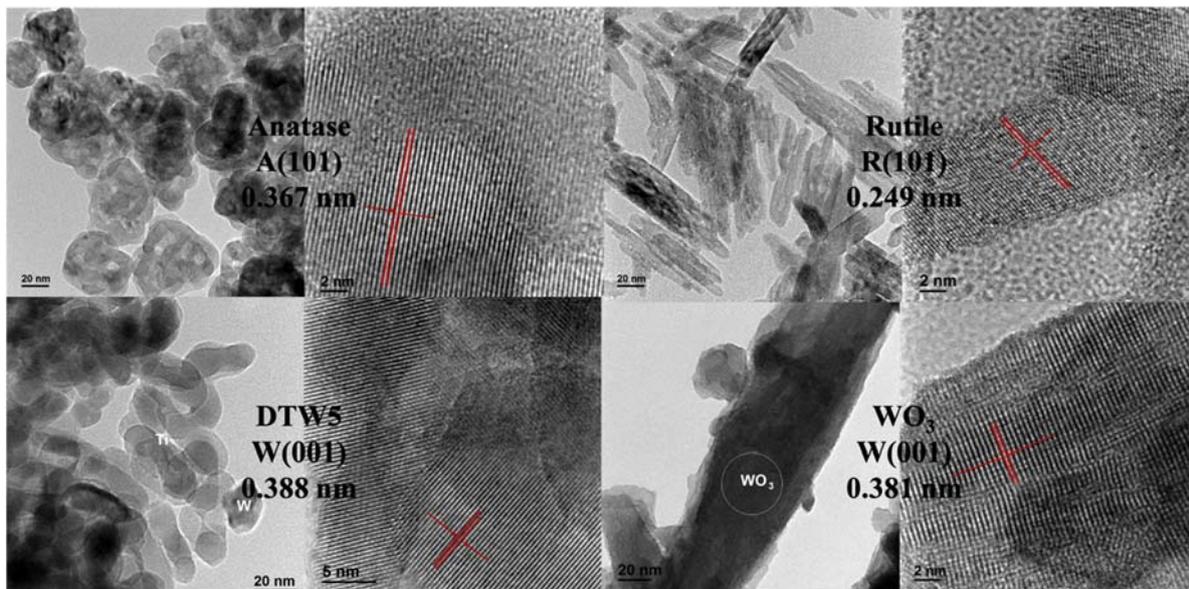
Fig. 2. High-resolution transmission electron microscopy (HRTEM) images of Anatase, Rutile, DTW5 and as-prepared WO₃ catalysts

Table 1. BET specific surface area, pore volume, pore size, crystallinity and average crystallite size of the photocatalysts

Sample	S_{BET} (m^2 g^{-1})	Porous volume (cm^3 g^{-1})	Mean Pore Size (nm)	Crystallinity[a] (%)	Crystal size[a] (nm)
Anatase	92	0.43	15.2	82.0	17
Rutile	85	0.39	16.9	80.8	16
P25	63	0.17	10.5	81.6	23 (Anatase)
DTW5	78	0.31	13.8	84.9	20 (Anatase)
WO$_3$	33	0.07	13.3	48.6	17

[a]Calculated from XRD spectra
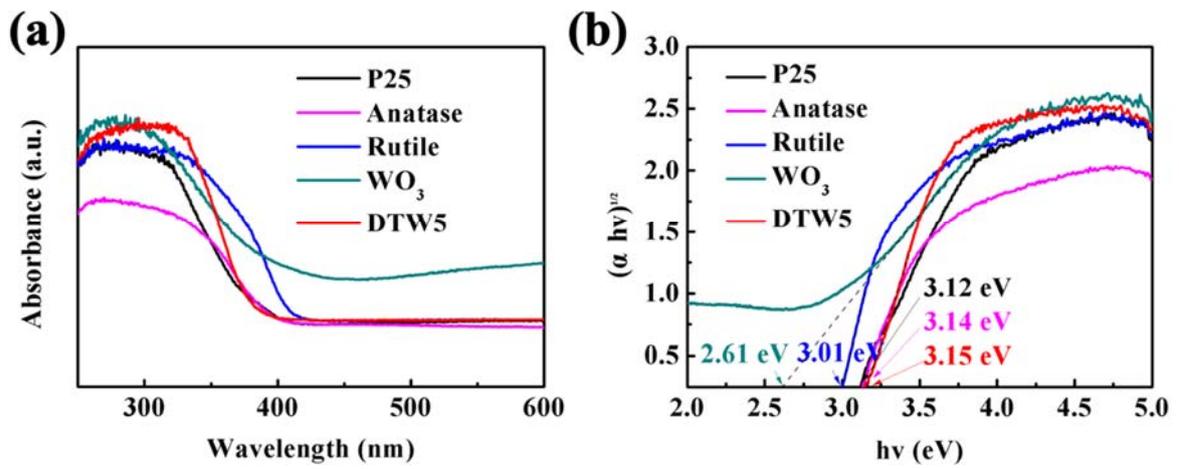
Fig. 3. (a) UV-Vis diffuse reflectance spectroscopy (DRS) spectra and (b) Tauc plot for band gap determination for commercial catalysts (Anatase, Rutile, P25 and DTW5) and as-prepared WO_3
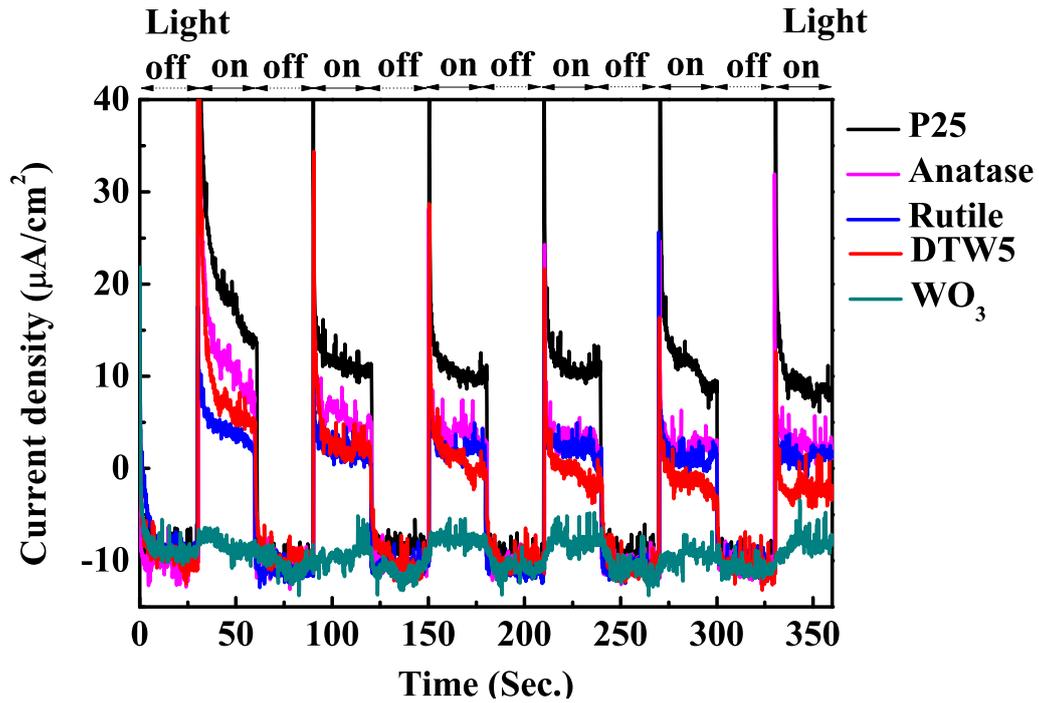
Fig. 4. Transient photocurrent response for commercial catalysts (Anatase, Rutile, P25 and DTW5) and as-prepared WO_3. Conditions: neutral reaction media (0.5 M Na2SO4), applied potential: 0.9 V vs Ag/AgCl. The experiments were performed in a photoelectrochemical cell, where the catalyst was supported on an ITO glass (working electrode), and a Pt counter electrode was used for polarization purposes.
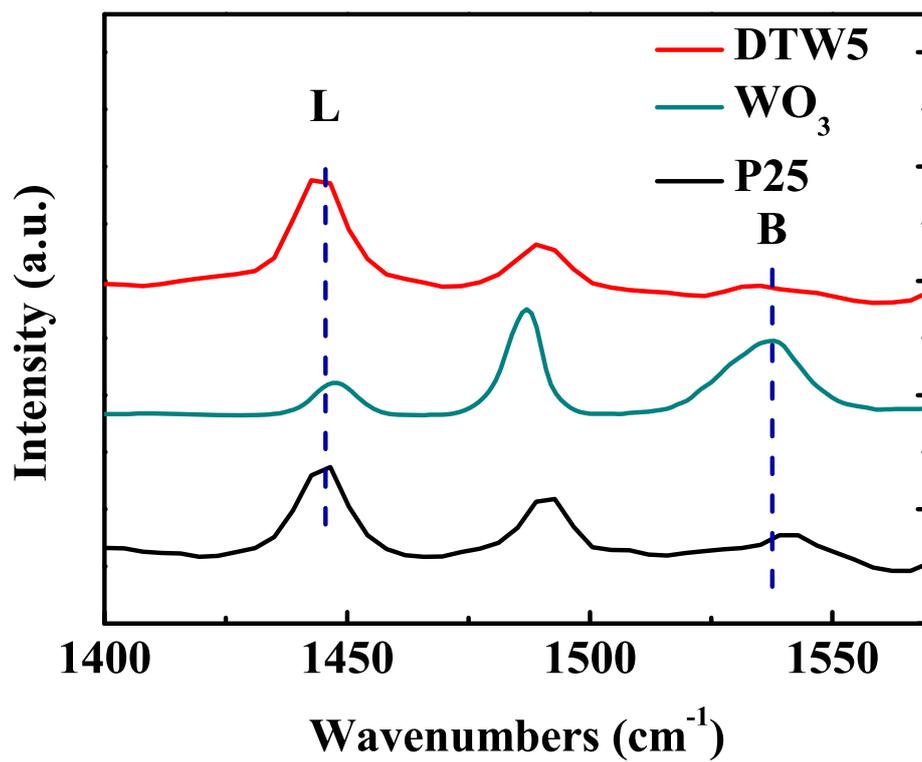
Fig. 5. pyridine-DRIFTS spectra of P25, DTW5 and WO₃. B and L denote Brönsted and Lewis acid sites, respectively.

Table 2. Comparison of Lewis, Brönsted and total acid sites of P25, DTW5 and WO_3, obtained by pyridine-DRIFTS

| Catalyst | μmol Py $\cdot$ g^{-1} $\cdot$ m^{-2} Cat. | | | |
	Lewis	Brönsted	Total	L/B
P25	0.87	0.21	1.08	4.2
DTW5	0.95	0.50	1.45	1.9
WO_3	0.64	3.33	3.97	0.2
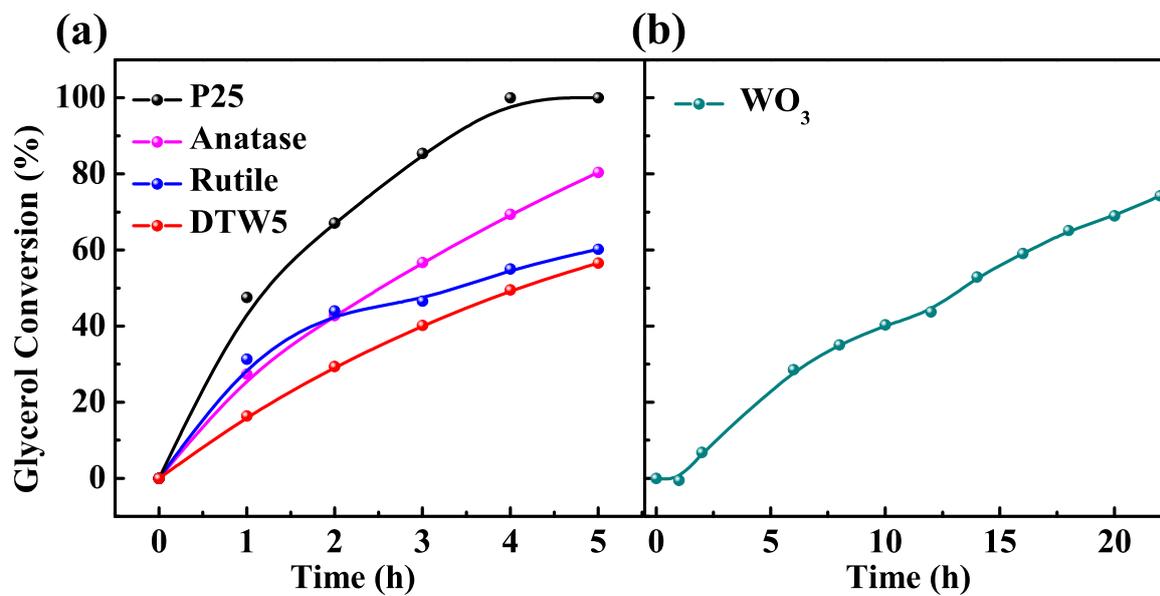
Fig. 6. Glycerol conversion over commercial catalysts (Anatase, Rutile, P25 and DTW5) and as-prepared WO$_3$. Reaction conditions: Room temperature, Glycerol initial concentration: 1.10 mmol L^{-1}, Volume of glycerol solution: 30 mL, UV irradiation intensity of 5.60 mW cm^2
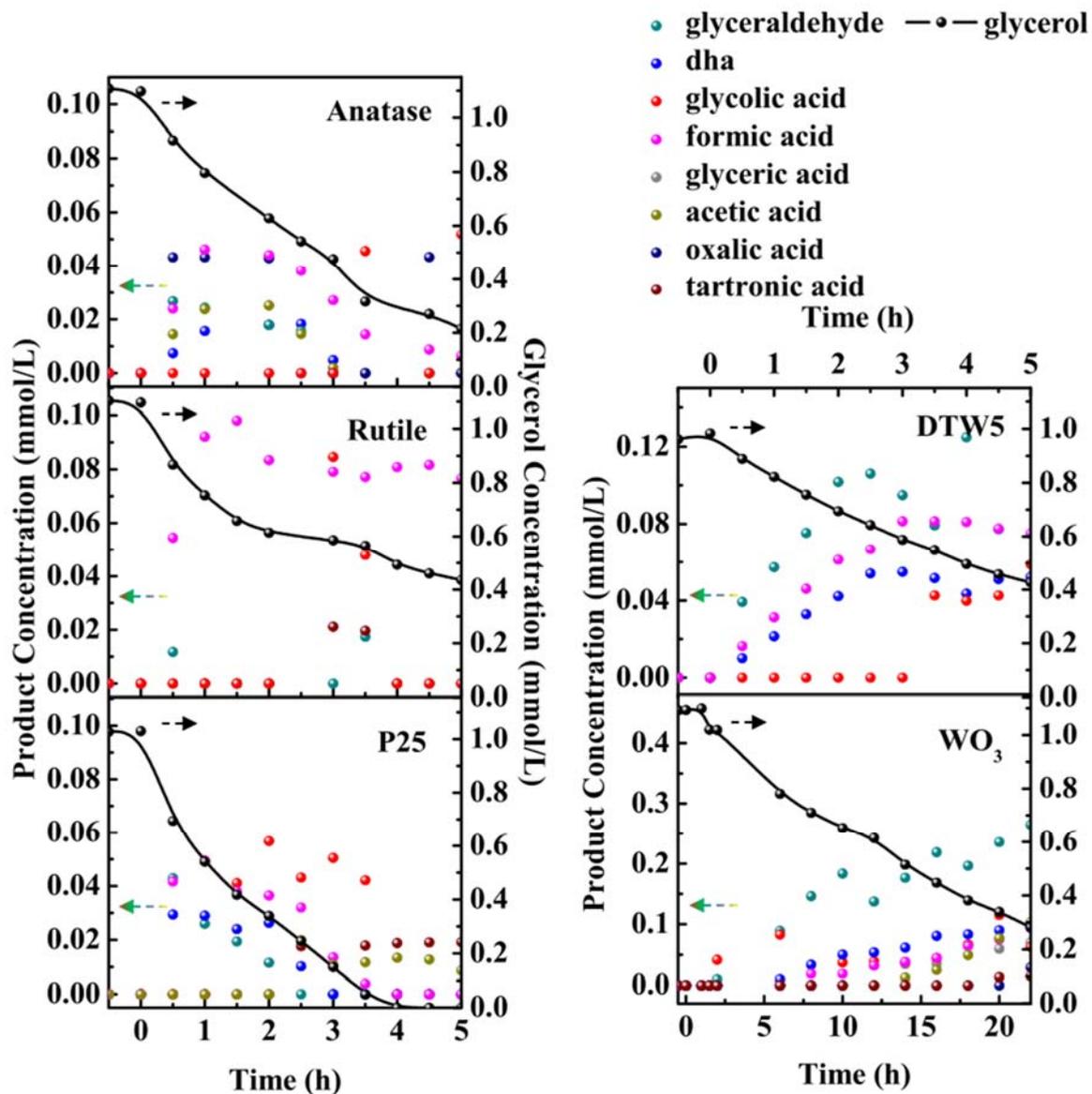
Fig. 7. Evolution of products with time over commercial catalysts (Anatase, Rutile, P25 and DTW5) and as-prepared WO₃. Reaction conditions: Room temperature, Glycerol initial concentration: 1.10 mmol L⁻¹, Volume of glycerol solution: 30 mL, UV irradiation intensity of 5.60 mW cm⁻²
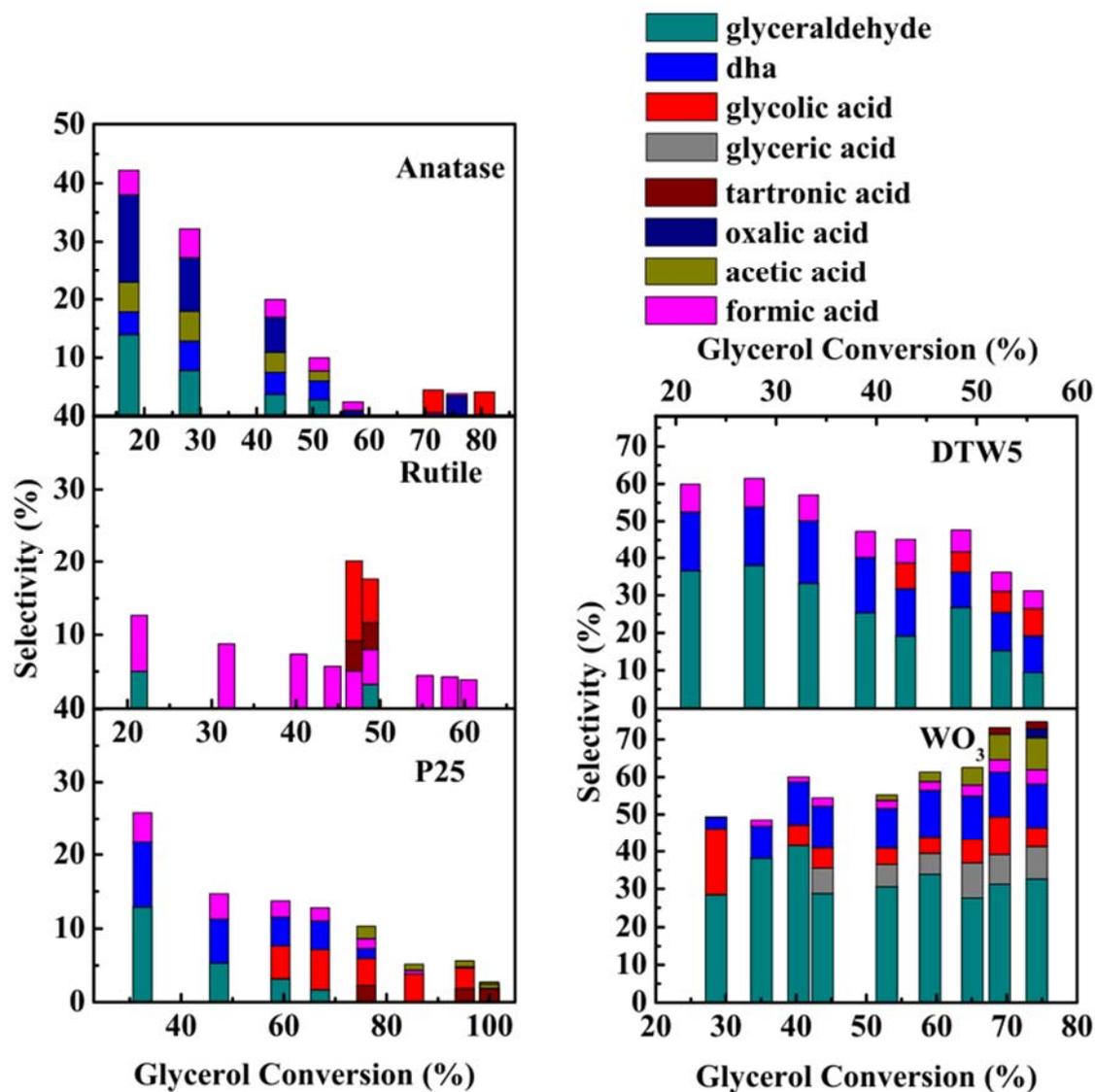
Fig. 8. Variation of products selectivity with respect to the glycerol conversion over commercial catalysts (Anatase, Rutile, P25 and DTW5) and as-prepared WO₃. Reaction conditions: Room temperature, Glycerol initial concentration: 1.10 mmol L^{-1}, Volume of glycerol solution: 30 mL, UV irradiation intensity of 5.60 mW cm^{-2}
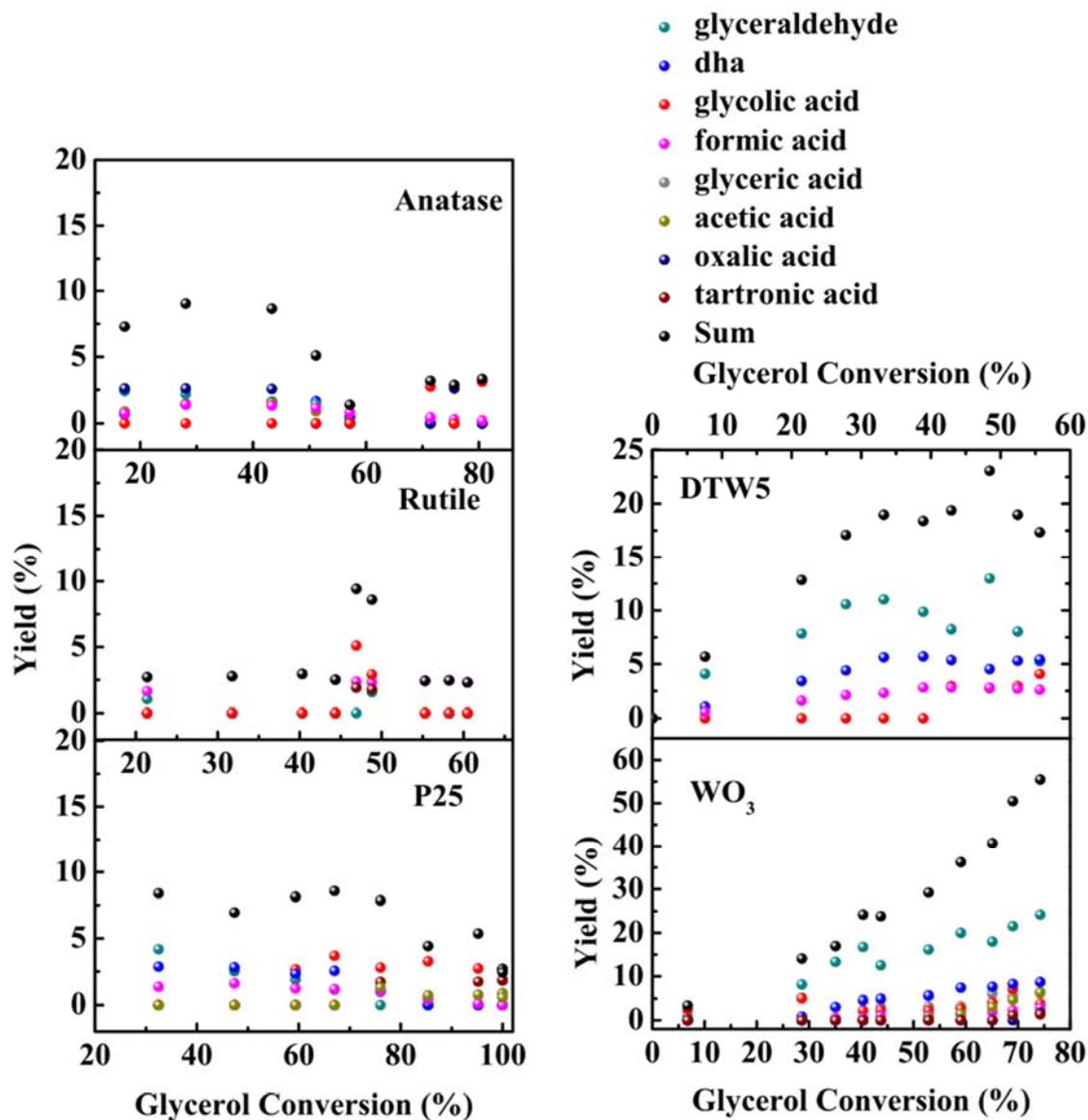
Fig. 9. Variation of products yield with respect to the glycerol conversion over commercial catalysts (Anatase, Rutile, P25 and DTW5) and as-prepared WO$_3$. Reaction conditions: Room temperature, Glycerol initial concentration: 1.10 mmol L^{-1}, Volume of glycerol solution: 30 mL, UV irradiation intensity of 5.60 mW cm^{-2}
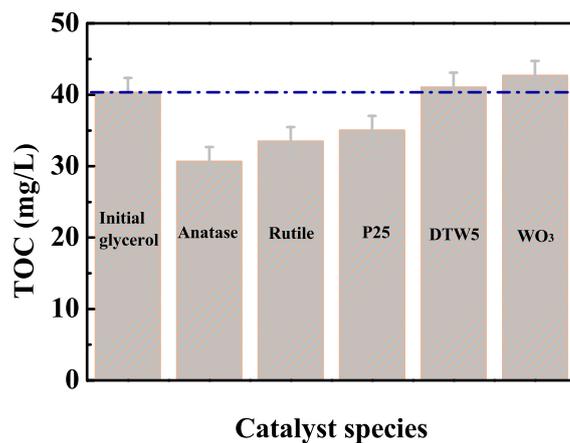
Fig. 10. Total organic carbon (TOC) measurement of the liquid solutions for commercial catalysts (Anatase, Rutile, P25 and DTW5) and as-prepared WO_3, after the achieved glycerol conversion was ~45 %. Reaction conditions: Room temperature, Glycerol initial concentration: 1.10 mmol L^{-1} (TOC: 40.4 ± 2 mg/L), Volume of glycerol solution: 30 mL, UV irradiation intensity of 5.60 mW cm^{-2}

Table 3. Comparison of glyceraldehyde Yield and Selectivity for all the photocatalysts at similar levels of glycerol conversion

Sample	Glycerol conversion (%)	Yield of glyceraldehyde (%)	Selectivity to glyceraldehyde (%)
Anatase	43	2	4
Rutile	44	/	/
P25	47	3	5
DTW5	43	8	19
WO_3	44	13	29
Homogeneous TiO_2 [27]	35	5	13
P25 [28]	36	5	13
Lab-made TiO_2 [53]	97	5	5
Black TiO_2 [54]	92	3	3